Hydrodynamic performance of a composite breakwater with an upper horizontal porous plate and a lower rubble mound

Yong Liu [*] and Hua-jun Li

Shandong Provincial Key Laboratory of Ocean Engineering, Ocean University of China, Qingdao 266100, China

Abstract. A composite breakwater with an upper horizontal porous plate and a lower rubble mound is proposed and studied in this work. By means of matched eigenfunction expansions, a semi-analytical solution is developed for analyzing the hydrodynamic performance of the breakwater. The semi-analytical solution is verified by known solutions for special cases and an independently developed multi-domain boundary element method solution. Numerical examples are given to examine the reflection, transmission and energy loss coefficients of the breakwater and the wave force acting on the horizontal porous plate. Some useful results are presented for engineering applications.

1. Introduction

A submerged horizontal porous plate supported by piles can be used as an offshore breakwater to provide shelter for coastlines and coastal structures. The vertical wave force acting on a porous plate is small as the plate is perforated. Also the transmission coefficient and the reflection coefficient may be both small with suitable designs (Yu and Chwang 1994, Neves *et al*. 2000). The small transmission coefficient is of significance for the shelter of leeside regions, and the small reflection coefficient is beneficial to reducing the seabed scouring in front of the breakwater and ensuring the safe navigation of vessels near the structure. Besides good hydrodynamic performance, the horizontal plate breakwater allows the free exchange of seawater between shelter and open regions, and thus prevents the seawater pollution.

A single horizontal plate must be installed near the free surface for effectively dissipating the incident wave energy (Yu and Chwang 1994). But the single horizontal plate fixed near the free surface can not meet the acute change of the still water level due to tide. One of solutions is to adopt multi-layer horizontal plates (Wang and Shen 1999, Wang *et al*. 2006, Liu *et al*. 2008, Kee 2009). However, the construction of multi-layer plates may be more difficult and the corresponding engineering cost may increase a lot. In this study, we provide an alternative solution by developing a composite breakwater with an upper horizontal porous plate and a low rubble mound (See Fig. 1). For the new composite breakwater, the horizontal porous plate can effectively

---

[*]Corresponding author, Ph.D, E-mail: liuyong_77@hotmail.com

dissipate the incident wave energy at the high still water level, and the submerged rubble mound can dissipate the incident wave energy at the low still water level. Thus the composite breakwater is always efficient at different still water levels. In addition, the free exchange of seawater between open and shelter regions is always ensured.

The objective of this study is to develop a semi-analytical solution for wave motion over the new composite breakwater and give more understanding for the hydrodynamic performance of the breakwater. Here the rubble mound is idealized as a rectangular bar for analytical study as usual. The case that the upper plate and the lower rubble mound are both submerged in the sea is considered in this study. At the low still water level, only the rubble mound is submerged in the sea. Analytical solutions for this special case have been given by Lee and Liu (1995), Losada *et al.* (1996) and Twu *et al.* (2001). Also, this special case can be recovered in the present solution by perforating the horizontal plate entirely (the upper plate disappears).

The boundary value problem for wave motion over the composite breakwater is formulated in the following Section and solved by matched eigenfunction expansions in Section 3. In Section 4, the newly developed solution is verified by previously known solutions for special cases and a multi-domain boundary element method (BEM) solution. Numerical examples with some useful results for practical engineering are given in Section 5. Finally the main conclusions are drawn.
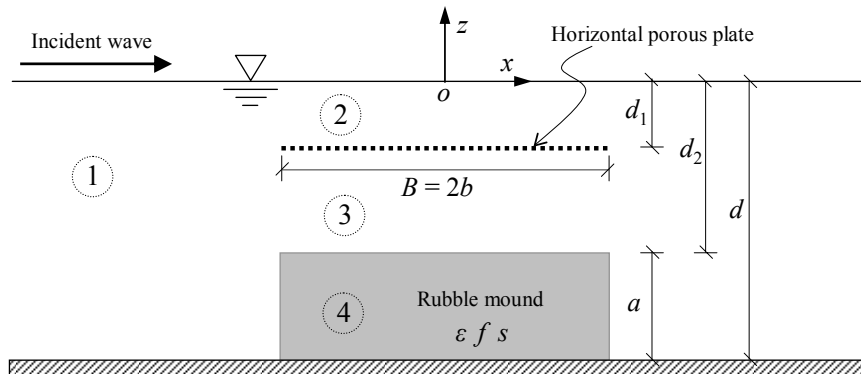

Fig. 1 Idealized sketch for wave scattering by a composite breakwater with an upper horizontal porous plate and a lower rubble mound

2. Boundary value problem

The idealized sketch for wave scattering by a composite breakwater including an upper horizontal porous plate and a lower rubble mound is given in Fig. 1. The composite breakwater is located in the sea with constant depth d. The submerged depths of the horizontal porous plate and the rubble mound are d_1 and d_2, respectively. The width of the breakwater is B (= $2b$), and the thickness of the rubble mound is a. The breakwater is subject to normally incident regular waves with the wave height H and the wavelength L. A Cartesian coordinate system, with the origin at the intersection of the still water level and the breakwater midline and the z-axis vertical upward, is used for mathematical descriptions.

The thickness of the porous plate is assumed to be zero as it is very small compared to the incident wavelength and the water depth. The rubble mound is assumed to be a rigid and homogenous porous medium. The present wave scattering problem is solved in the context of the linear potential theory and the classical porous medium model of Sollitt and Cross (1972). Then, a velocity potential is used to describe fluid motions in the whole domain (including the rubble mound region). By further considering harmonic waves with angular frequency ω, a time factor $\exp(-i\omega t)$ is separated from the velocity potential. Only a spatial velocity potential ϕ independent of time needs to be determined.

The velocity potential ϕ satisfies the Laplace equation

$$\frac{\partial^2 \phi(x,z)}{\partial x^2} + \frac{\partial^2 \phi(x,z)}{\partial z^2} = 0 \tag{1}$$

The velocity potential also satisfies boundary conditions on the free surface, the seabed and the far fields

$$\frac{\partial \phi}{\partial z} = K\phi, \qquad K = \omega^2 / g \quad , \qquad z = 0 \tag{2}$$

$$\frac{\partial \phi}{\partial z} = 0 \quad , \qquad z = -d \tag{3}$$

$$\lim_{x \to \pm\infty} \left(\frac{\partial}{\partial x} \mp ik_0 \right) \binom{\phi}{\phi - \phi^I} = 0 \tag{4}$$

where g is the gravitational acceleration; k_0 is the incident wave number; and ϕ^I is the velocity potential of incident waves.

On the horizontal porous plate, the velocity potential satisfies following velocity and pressure transmission conditions (Yu 1995)

$$\frac{\partial \phi^+}{\partial z} = \frac{\partial \phi^-}{\partial z} = ik_0 G\left(\phi^- - \phi^+\right) \quad , \quad z = -d_1 , \quad |x| \le b \tag{5}$$

where G is the porous effect parameter of the porous plate (Yu 1995); and the superscripts $+$ and $-$ denote, respectively, the values on the upper and lower sides of the plate. When G is zero, the plate becomes a solid plate. While G approaches infinity, the horizontal porous plate disappears. The value of G increases with the increasing geometrical porosity of the porous plate. In practice, the value of G must be determined by experimental tests. The boundary condition in Eq. (5) denotes that on the porous plate surface, the normal fluid velocity is continuous and linearly proportional to the pressure jump between the two sides of the plate.

On the common boundary of the rubble mound and surrounding fluids, the velocity and pressure transmission conditions are given by (Sollitt and Cross 1972)

$$\frac{\partial \phi^+}{\partial n} = \varepsilon \frac{\partial \phi^-}{\partial n}$$

(6)

$$\phi^+ = (s + \mathrm{i}f)\phi^-$$

(7)

where the superscripts + and − denote, respectively, the values outside and inside the rubble mound; n is the unit normal vector on the rubble mound surface; and the symbols ε, s and f are, respectively, the porosity, the inertial coefficient and the linearized resistance coefficient of the rubble mound (Sollitt and Cross 1972). If $\varepsilon = 1$, $s = 1$ and $f = 0$, the porous medium will become water. Generally, the inertial coefficient s may be simply treated as unity. But the resistance coefficient f should be iteratively calculated by the Lorentz's hypothesis of equivalent work in practical applications (Sollitt and Cross 1972).

The Eqs. (1) - (7) formulate a complete boundary value problem. It is solved by matched eigenfunction expansions in the next Section.

3. Matched eigenfunction expansions

For simplicity of solution, we split the velocity potential into a symmetric part and an antisymmetric part (Mei and Black 1969, Fernyhough and Evans 1995)

$$\phi(x,z) = \frac{1}{2}\left[\phi^S(x,z) + \phi^A(x,z)\right]$$

(8)

where

$$\phi^S(-x,z) = \phi^S(x,z)$$

(9a)

$$\phi^A(-x,z) = -\phi^A(x,z)$$

(9b)

It is evident that the symmetric and antisymmetric potentials still satisfy the Laplace equation and the relevant boundary conditions described in Section 2. We only need solve this problem in the left half plane ($x \leq 0$), and then extend the solution to the right half plane by the symmetric and antisymmetric relations in Eq. (9).

We only detail the symmetric problem and then describe the necessary changes in the antisymmetric problem. As shown in Fig. 1, the left half plane is divided into four regions: region 1, the fluid domain in front of the composite breakwater; region 2, the fluid domain above the horizontal porous plate; region 3, the fluid domain between the plate and the rubble mound; and region 4, the fluid domain inside the rubble mound.

In the region 1, the symmetric potential ϕ_1^S, satisfying the Laplace equation in Eq. (1) and the boundary conditions in Eqs. (2) - (4), can be written as

$$\phi_1^S = -\frac{\mathrm{i}gH}{2\omega}\left[\mathrm{e}^{\mathrm{i}k_0(x+b)}Z_0(z) + R_0\mathrm{e}^{-\mathrm{i}k_0(x+b)}Z_0(z) + \sum_{n=1}^{\infty}R_n\mathrm{e}^{k_n(x+b)}Z_n(z)\right]$$

(10)

where R_n are unknown expansion coefficients; and $Z_n(z)$ are vertical eigenfunctions given by

$$Z_0(z) = \cosh k_0(z + d)/\cosh k_0 d \tag{11a}$$

$$Z_n(z) = \cos k_n(z + d)/\cos k_n d \ , \quad n = 1, 2, \dots \tag{11b}$$

in which the wave numbers k_n are the positive roots of following dispersion relations

$$K = k_0 \tanh k_0 d = -k_n \tan k_n d \ , \quad n = 1, 2, \dots, \tag{12}$$

In the regions 2 – 4, we decompose the symmetric potentials as

$$\phi_j^S = \phi_j^{S,h} + \phi_j^{S,v} \ , \quad j = 2, 3, 4 \tag{13}$$

where the subscript j denotes the values in the region j. The decomposed potentials $\phi_j^{s,h}$ and $\phi_j^{S,v}$ still satisfy the Laplace equation in Eq. (1) and the relevant boundary conditions in Eqs. (2) and (3). According to Eq. (9(a)), the decomposed potentials satisfy

$$\frac{\partial \phi_j^{S,h}}{\partial x} = 0, \quad x = 0, \quad j = 2, 3, 4 \tag{14}$$

$$\frac{\partial \phi_j^{S,v}}{\partial x} = 0, \quad x = 0, \quad j = 2, 3, 4 \tag{15}$$

We further make the decomposed potentials satisfy

$$\phi_j^{S,h} = 0, \quad x = -b, \quad j = 2, 3, 4 \tag{16}$$

$$\frac{\partial \phi_j^{S,v}}{\partial z} = 0, \quad z = -d_1, \quad j = 2, 3 \tag{17}$$

$$\frac{\partial \phi_j^{S,v}}{\partial z} = 0, \quad z = -d_2, \quad j = 3, 4 \tag{18}$$

Then, the decomposed potentials in regions 2 - 4, which satisfy the Laplace equation in Eq. (1) and the relevant boundary conditions in Eqs. (2), (3) and (14) - (18), can be written as

$$\phi_2^{S,v} = -\frac{igH}{2\omega} \left[A_0 \cos(\lambda_0 x) Y_n(z) + \sum_{n=1}^{\infty} A_n \frac{\cosh \lambda_n x}{\cosh \lambda_n b} Y_n(z) \right] \tag{19}$$

$$\phi_3^{S,v} = -\frac{igH}{2\omega}\left[B_0 V_0(z) + \sum_{n=1}^{\infty} B_n \frac{\cosh \upsilon_n x}{\cosh \upsilon_n b}V_n(z)\right] \tag{20}$$

$$\phi_4^{S,v} = -\frac{igH}{2\omega}\left[C_0 X_0(z) + \sum_{n=1}^{\infty} C_n \frac{\cosh \mu_n x}{\cosh \mu_n b}X_n(z)\right] \tag{21}$$

$$\phi_2^{S,h} = -\frac{igH}{2\omega}\sum_{n=0}^{\infty} D_n W_n(x)\frac{\cosh \beta_n z + (K/\beta_n)\sinh \beta_n z}{\cosh \beta_n d_1} \tag{22}$$

$$\phi_3^{S,h} = -\frac{igH}{2\omega}\sum_{n=0}^{\infty} W_n(x)\frac{E_n \cosh \beta_n (z+d_1+a_1) + F_n \sinh \beta_n (z+d_1+a_1)}{\cosh \beta_n a_1} \tag{23}$$

$$\phi_4^{S,h} = -\frac{igH}{2\omega}\sum_{n=0}^{\infty} G_n W_n(x)\frac{\cosh \beta_n (z+d)}{\cosh \beta_n a} \tag{24}$$

where, $a_1 = (d_2 - d_1)/2$; $A_n, B_n, C_n, D_n, E_n, F_n$ and G_n are unknown expansion coefficients; and the vertical eigenfunctions $Y_n(z)$, $V_n(z)$ and $X_n(z)$ and the horizontal eigenfunctions $W_n(x)$ are given by

$$Y_0(z) = \cosh \lambda_0 (z+d_1)/\cosh \lambda_0 d_1 \tag{25a}$$

$$Y_n(z) = \cos \lambda_n (z+d_1)/\cos \lambda_n d_1 \text{,} \quad n = 1,2,\ldots \tag{25b}$$

$$V_0(z) = \sqrt{2}/2 \tag{26a}$$

$$V_n(z) = \cos \upsilon_n (z+d_2) \text{,} \quad n = 1,2,\ldots \tag{26b}$$

$$X_0(z) = \sqrt{2}/2 \tag{27a}$$

$$X_n(z) = \cos \mu_n (z+d) \text{,} \quad n = 1,2,\ldots \tag{27b}$$

$$W_n(x) = \cos \beta_n x \text{,} \quad n = 0,1,2,\ldots \tag{28}$$

in which the eigenvalues are determined by

$$K = \lambda_0 \tanh \lambda_0 d_1 = -\lambda_n \tan \lambda_n d_1 \text{,} \quad n = 1,2,\ldots \tag{29}$$

$$\upsilon_n = n\pi / (d_2 - d_1), \quad n = 1,2,\dots \tag{30}$$

$$\mu_n = n\pi / a, \quad n = 1,2,\dots \tag{31}$$

$$\beta_n = (n + 0.5)\pi / b, \quad n = 0,1,2,\dots \tag{32}$$

We note that the eigenfunctions in Eqs. (25) - (28) are all orthogonal in their own intervals.

Now the velocity potentials in all the regions have been given in terms of series expansions with unknown coefficients. We must use the boundary conditions in Eqs. (5) - (7) to determine the unknown coefficients. For example, inserting the relevant velocity potentials into the first part in Eq. (5), multiplying both sides of equals sign by $W_n(x)$ and integrating with respect to x from $-b$ to 0, then using the orthogonality of $W_n(x)$ and truncating n to N, we have

$$D_n = \frac{E_n \tanh \beta_n a_1 + F_n}{K/\beta_n - \tanh \beta_n d_1}, \quad n = 0,1,2,\dots,N \tag{33}$$

The second part in Eq. (5) and Eqs. (6) and (7) are conducted by the similar method. Then, we obtain another seven sets of linear equations, which are given in Appendix A. All the unknown expansion coefficients are determined by simultaneously solving the eight sets of linear equations.

We note that in physics, the above symmetric problem is equal to setting a solid vertical wall at the midline of the breakwater. This is significant for designing a porous wave absorber attached to the end wall of a wave flume or a vertical seawall (Cho and Kim 2008, Yueh and Chuang 2009).

We also note that the velocity potentials in regions 2 - 4 may be directly written out by simultaneously considering the free surface condition in Eq. (2), the seabed condition in Eq. (3) and the boundary conditions in Eqs. (5) - (7). An example for directly constructing velocity potentials in dissipative regions can be found in Neves *et al.* (2000). However, a complicated complex dispersion relation is encountered. The accurate numerical solution for such a complex dispersion relation is very difficult. This difficulty has been overcome by the present velocity potential decomposition procedure, as given in Eqs. (13) - (18). The velocity potential decomposition procedures for other dissipative (porous) structures can be found in Lee and Liu (1995), Lan and Li (2010), Lan *et al.* (2011) and Liu *et al.* (2012).

For the antisymmetric problem, a similar procedure with following changes is performed. Eqs. (14) - (16) are modified as

$$\phi_j^{A,h} = 0, \quad x = 0, \quad j = 2,3,4 \tag{34}$$

$$\phi_j^{A,v} = 0, \quad x = 0, \quad j = 2,3,4 \tag{35}$$

$$\frac{\partial \phi_j^{A,h}}{\partial x} = 0, \quad x = -b, \quad j = 2,3,4 \tag{36}$$

As a result, the cosine and cosh functions with respect to x in Eqs. (19) - (21) are replaced by sine

and sinh functions, respectively. The first term in Eqs. (20) and (21) is multiplied by a factor of x, and the function $\cos \beta_n x$ in Eq. (28) is replaced by $\sin \beta_n x$.

We rewrite the expansion coefficient R_n in the symmetric and antisymmetric potentials as R_n^S and R_n^A, respectively. The reflection coefficient C_R, the transmission coefficient C_T and the energy loss coefficient C_L of the composite breakwater are calculated by

$$C_R = \frac{\left| R_0^S + R_0^A \right|}{2} \tag{37}$$

$$C_T = \frac{\left| R_0^S - R_0^A \right|}{2} \tag{38}$$

$$C_L = 1 - C_R^2 - C_T^2 \tag{39}$$

The vertical wave force acting on the horizontal porous plate is obtained by integrating the dynamic pressure along the plate surface

$$
F = \mathrm{i}\rho\omega \int_{-b}^{b} (\phi_3 - \phi_2)\big|_{z=-d_1}\, \mathrm{d}x = \mathrm{i}\rho\omega \int_{-b}^{0} (\phi_3^S - \phi_2^S)\big|_{z=-d_1}\, \mathrm{d}x
$$

$$
= \frac{\rho\omega}{k_0 G} \int_{-b}^{0} \frac{\partial \phi_2^{S,h}}{\partial z}\bigg|_{z=-d_1}\, \mathrm{d}x = \frac{\rho g H}{\mathrm{i}2 k_0 G} \sum_{n=0}^{N} D_n \left(K/\beta_n - \tanh \beta_n d_1 \right) \sin \beta_n b \tag{40}
$$

where we have used the Bernoulli equation $p(x,z) = i\rho\omega\phi(x,z)$ (p is the dynamic pressure and ρ is the water density) and the boundary conditions in Eq. (5). The expansion coefficients D_n in Eq. (40) are that in Eq. (22) for the symmetric solution. The dimensionless vertical force is defined as

$$C_F = \frac{|F|}{\rho g H B} \tag{41}$$

We note that to ensure the convergence of the series solution, the value of the truncated number N used in calculations must be carefully determined. We have found that $N = 40$ is enough for obtaining satisfactory results of hydrodynamic quantities. In the following calculations, the value of $N = 40$ is used.

4. Validations

We first examine two special cases of the present solution. When the porous effect parameter G of the plate increases to infinity, the plate disappears and the present breakwater becomes a submerged rectangular porous bar. For this special case, our results of reflection and transmission

coefficients are the same as those by the analytical solution of Twu *et al.* (2001). This is shown in Fig. 2 at $G \to \infty$, $d_2/d = 0.5$, $B/d = 1.0$, $\varepsilon = 0.3$, $s = 1.0$ and $f = 1.0$. When $\varepsilon = 1.0$, $s = 1.0$ and $f = 0$, the rubble mound disappears and the present breakwater becomes a single horizontal porous plate. For this special case, our present results are the same as those by the analytical solution of Yip and Chwang (1998), which is not plotted here for simplicity.
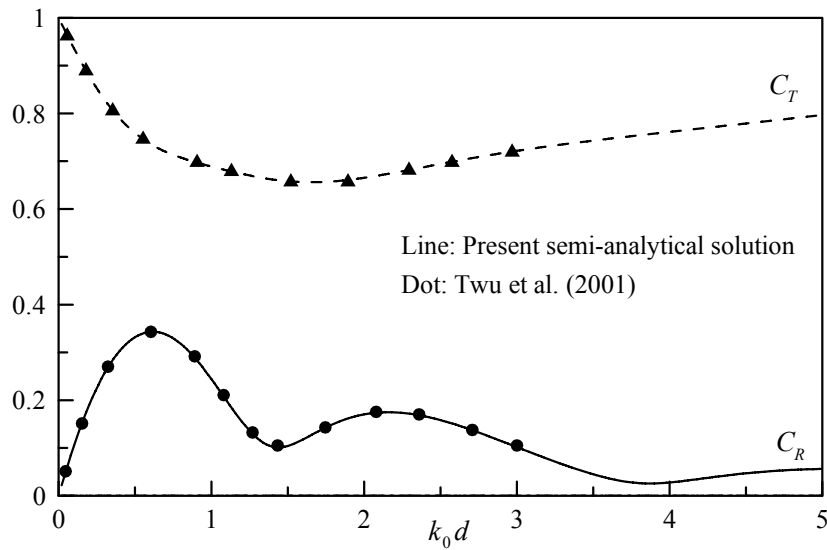

Fig. 2 Comparison between the present solution and Twu *et al.* (2001) at: $G \to \infty$, $d_2/d = 0.5$, $B/d = 1.0$, $\varepsilon = 0.3$, $s = 1.0$ and $f = 1.0$

(a) $G = 0.5$ (b) $G = 1.0$
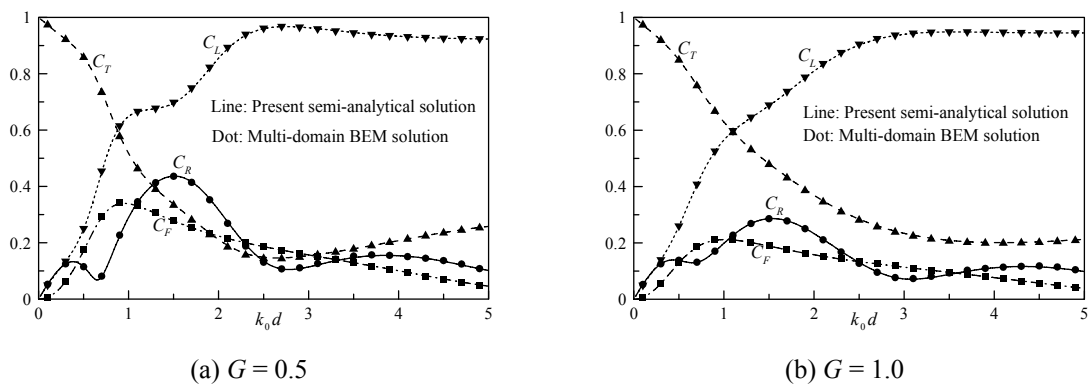
Fig. 3 Comparison between the present semi-analytical solution and the multi-domain BEM   solution at: $d_1/d = 0.1$, $d_2/d = 0.5$, $B/d = 1.0$, $\varepsilon = 0.45$, $s = 1.0$ and $f = 2.0$

The present boundary value problem has also been solved using multi-domain BEM (Liu *et al.* 2012). The multi-domain BEM solution is efficient for more general structure shapes, such as a trapezoidal rubble mound. Fig. 3 gives a comparison between the present semi-analytical solution and the multi-domain BEM solution. The calculating conditions are: $d_1/d = 0.1$, $d_2/d = 0.5$, $B/d = 1.0$, $\varepsilon = 0.45$, $s = 1.0$, $f = 2.0$ and $G = 0.5$ and 1.0, respectively. It can be seen from Fig. 3 that the agreement between the present semi-analytical solution and the multi-domain BEM solution is excellent.

The preceding comparisons indicate that the present semi-analytical solution should be valid.

5. Discussion

We give some numerical examples to examine the hydrodynamic performance of the composite breakwater.

Fig. 4 gives the effects of the porous effect parameter G on the hydrodynamic quantities of the breakwater. The calculating conditions are: $k_0 d = 1.5$, $d_1/d = 0.1$, $d_2/d = 0.4$, $\varepsilon = 0.45$, $s = 1.0$, $f = 2.0$ and $B/L = 0.4$ and 0.2, respectively. Each quantity is plotted as a function of G on a logarithmic scale. It can be seen from Fig. 4 that with the increasing G (the plate porosity), the reflection coefficient C_R and the dimensionless wave force C_F both decrease monotonously. But the energy loss coefficient C_L first increases, attains its maximum and then decreases. This has also been observed by Yu and Chwang (1994) for a single horizontal porous plate, and means that a porous plate with moderate porosity can dissipate more incident wave energy. We also note from Fig. 4 that with the increasing plate porosity, the transmission coefficient C_T first decreases, attains its minimum and then increases. This should be due to the combined effects of the wave reflection and the wave energy loss. In Fig. 4, the porous effect parameter G is about 0.6 when the energy loss coefficient attains maximum. At this time, the plate porosity P is about 8% according to the empirical formula of Cho and Kim (2008), which reads $G = (57.63P - 0.9717) / (2\pi)$. By considering both smaller transmission and reflection coefficients and smaller wave force acting on the plate, the plate porosity of 8% may be reasonable for the present breakwater. This should be of significance in practical designs. For a Jarlan-type perforated breakwater including a vertical perforated front wall and a solid rear wall, we have known that the optimum porosity of the perforated wall is about 20%, and may increase to 40% with the decreasing internal water depth (Huang *et al.* 2011). This is very different from the present breakwater.

The reflection, transmission and energy loss coefficients for the present composite breakwater, a single horizontal porous plate breakwater and a single rubble mound breakwater are compared in Fig. 5. The calculating conditions for the composite breakwater are: $k_0 d = 1.5$, $d_1/d = 0.1$, $d_2/d = 0.4$, $G = 0.6$, $\varepsilon = 0.45$, $s = 1.0$ and $f = 2.0$. For the single horizontal porous plate, we make $\varepsilon = 1.0$, $s = 1.0$ and $f = 0$. The other parameters are the same as that of the composite breakwater. For the single rubble mound, the value of G is infinity and the other parameters are the same as that of the composite breakwater. In Fig. 5, each hydrodynamic quantity is plotted as a function of the relative plate width (the ratio of the plate width B to the incident wavelength L). It can be seen from Figs. 5(b) and (c) that the composite breakwater has the maximum energy loss coefficient and the minimum transmission coefficient. So, the composite breakwater can provide better shelter for leeside regions. However the reflection coefficient of the composite breakwater is not always larger than that of other structures, as shown in Fig. 5(a). When the relative width of the structure

is smaller than 0.35, the reflection coefficient of the composite breakwater may be smaller than that of the single horizontal porous plate. This is an interesting phenomenon, which may be due to the fact that the interaction between the fluids upper and lower the porous plate is reduced by the rubble mound.
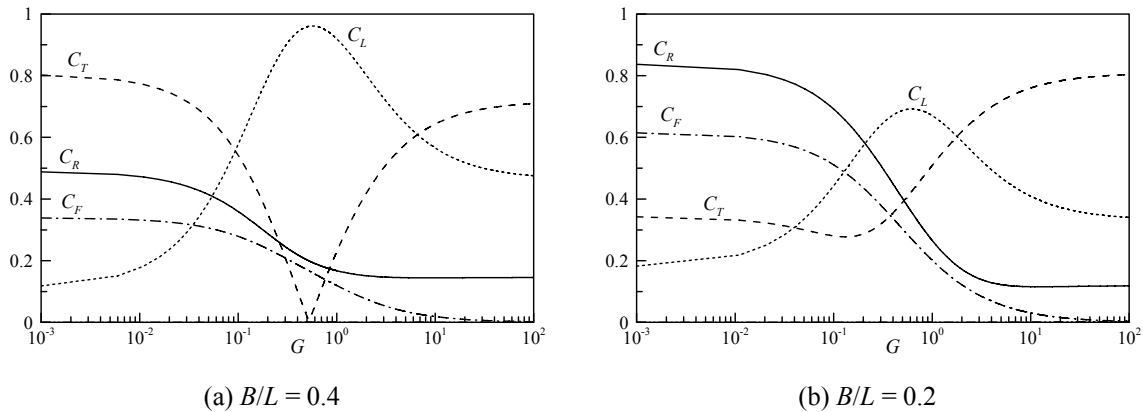

(a) $B/L = 0.4$ (b) $B/L = 0.2$

Fig. 4 Effects of the porous effect parameter G on the hydrodynamic quantities at: $k_0 d = 1.5$, $d_1/d = 0.1$, $d_2/d = 0.4$, $\varepsilon = 0.45$, $s = 1.0$ and $f = 2.0$

The dimensionless wave forces acting on the porous plate of the present composite breakwater and a single horizontal porous plate breakwater are compared in Fig. 6. Here the calculating conditions are the same as that in Fig. 5. It can be seen from Fig. 6 that when constructing a rubble mound below a horizontal porous plate, the wave force acting on the plate decreases. Then the stability of the horizontal porous plate is enhanced.

Finally, the effects of the relative submerged depth d_2/d of the rubble mound on C_T and C_F for the present composite breakwater are given in Fig. 7. The calculating conditions are: $k_0 d = 1.5$, $d_1/d = 0.1$, $G = 0.6$, $\varepsilon = 0.45$, $s = 1.0$ and $f = 2.0$. It can be seen from Fig. 7(a) that if the relative submerged depth of the rubble mound decreases (the thickness of the rubble mound increases), the transmission coefficient of the breakwater will not necessarily decrease. When the value of d_2/d decreases from 0.3 to 0.1, the transmission coefficient may increase a lot at $B/L = 0.3 - 0.5$. This means that if the design of the breakwater is not suitable, the shelter function of the breakwater will be reduced and the rubble materials will be wasted. The relative submerged depth of $d_2/d = 0.3 - 0.5$ is recommended for engineering applications. From Fig. 7(b), it is evident that the dimensionless wave force acting on the horizontal porous plate decreases with the deceasing submerged depth of the rubble mound. This is consistent with that observed in Fig. 6. It means that the rubble mound reduces the wave force acting on the plate, and then enhances the stability of the plate.

(a) Reflection coefficient C_R

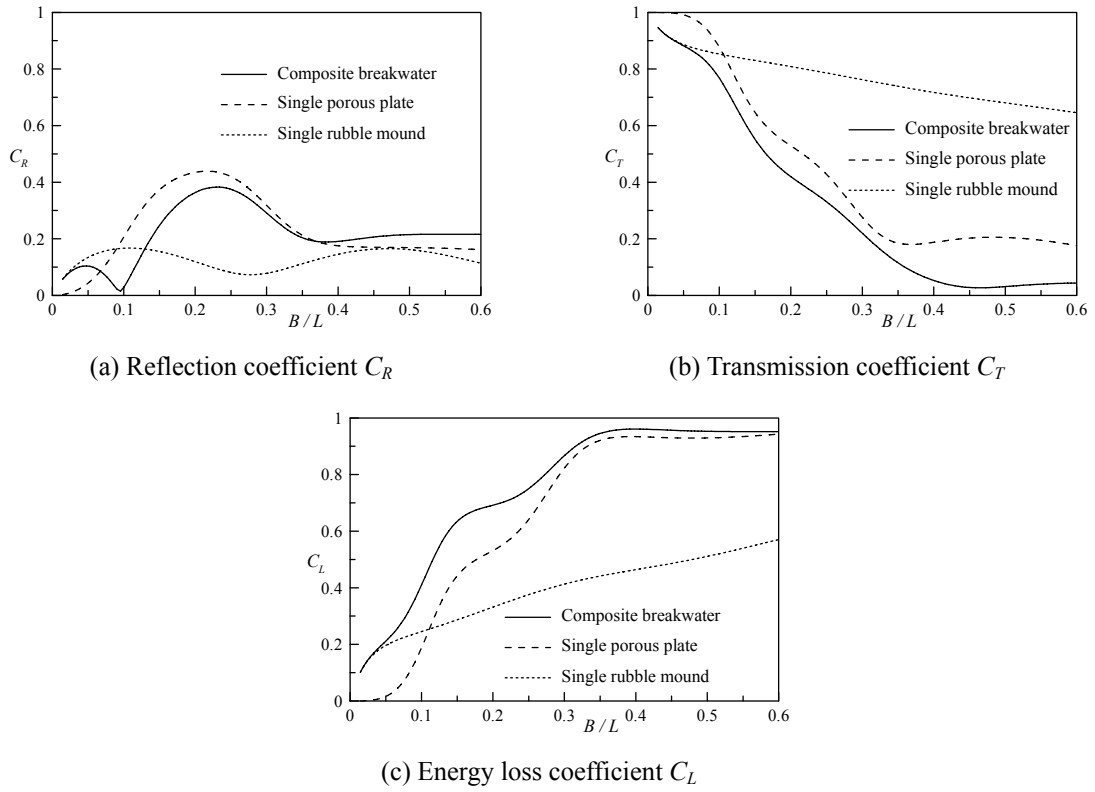(b) Transmission coefficient C_T

(c) Energy loss coefficient C_L

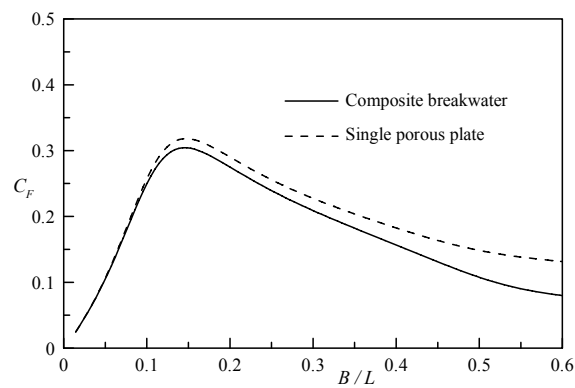Fig. 5 Comparisons of the reflection, transmission and energy loss coefficients among three different breakwaters

Fig. 6 Comparison of the dimensionless wave forces between the present composite breakwater and a single horizontal porous plate breakwater
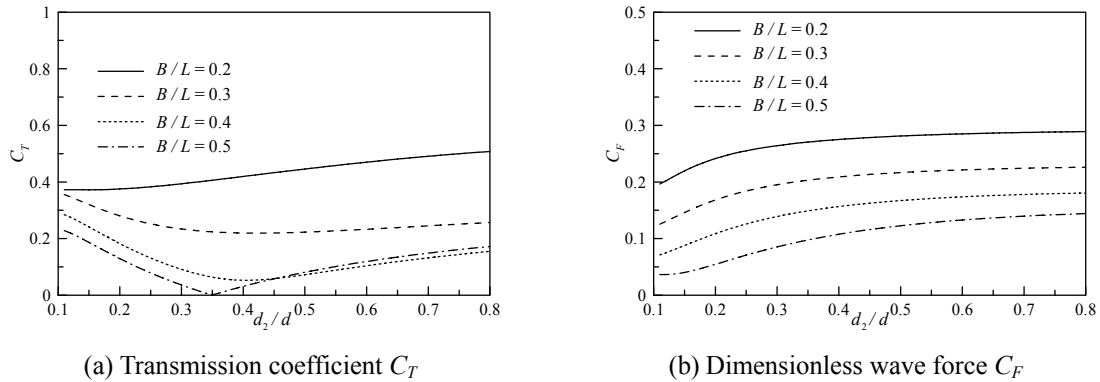
(a) Transmission coefficient C_T

(b) Dimensionless wave force C_F

Fig. 7 Effects of the relative submerged depth d_2/d of rubble mound on C_T and C_F at: $k_0 d = 1.5$, $d_1/d = 0.1$, $G = 0.6$, $\varepsilon = 0.45$, $s = 1.0$ and $f = 2.0$

6. Conclusions

A composite breakwater with an upper horizontal porous plate and a lower rubble mound has been proposed and studied. A semi-analytical solution for wave motion over the composite breakwater has been developed using matched eigenfunction expansions. The calculated results of the semi-analytical solution are the same as those by known solutions for a submerged porous bar and a single horizontal porous plate. The present semi-analytical solution has also been verified by a multi-domain BEM solution.

Numerical examples have indicated that the composite breakwater can provide better shelter in compared with a single horizontal porous plate or a single rubble mound. Adding a rubble mound below a horizontal porous plate can reduce the wave force acting on the plate and then enhance the stability of the plate. The submerged depth of the rubble mound must be carefully determined for providing better shelter. The ratio of the submerged depth of the rubble mound to the water depth is recommended as 0.3 - 0.5. The recommended value of the plate porosity is about 8%. By adopting these recommended values, the composite breakwater can dissipate more incident wave energy.

The present composite breakwater should be an effective offshore breakwater with small transmission coefficient and small wave force. Most of all, the composite breakwater can meet the acute change of the still water level and always guarantee the free exchange of seawater. Experimental studies on the composite breakwater may be carried out in the future.

Acknowledgments

References

Cho, I.H. and Kim, M.H. (2008), "Wave absorbing system using inclined perforated plates", *J. Fluid Mech.*, **608**, 1-20.

Fernyhough, M. and Evans, D.V. (1995), "Scattering by a periodic array of rectangular blocks", *J. Fluid Mech.*, **305**, 263-279.

Huang, Z.H., Li, Y. C. and Liu, Y. (2011), "Hydraulic performance and wave loadings of perforated/slotted coastal structures: A review", *Ocean Eng.*, **38**(10), 1031-1053.

Kee, S.T. (2009), "Submerged plate breakwater composed of horizontal porous plate and slightly inclined solid plate", *Int. J. Offshore Polar Eng.*, **19**(1), 42-45.

Lan, Y.J. and Lee, J.F. (2010), "On waves propagating over a submerged poro-elastic structure", *Ocean Eng.*, **37**, 705-717.

Lan, Y.J., Hsu, T.W., Lai, J.W., Chwang, C.C. and Ting, C.H. (2011), "Bragg scattering of waves propagating over a series of poro-elastic submerged breakwaters", *Wave Motion*, **48**(1), 1-12.

Lee, J. F. and Liu, C. C. (1995), "A new solution of waves passing a submerged porous structure", *Proceedings of the 17th Ocean Engineering Conference*, Taiwan, China. (in Chinese with English abstract)

Liu, Y., Li, H.J. and Li, Y.C. (2012), "A new analytical solution for wave scattering by a submerged horizontal porous plate with finite thickness", *Ocean Eng.*, **42**, 83-92.

Liu, Y., Li, Y. C., Teng, B. and Dong, S. (2008), "Wave motion over a submerged breakwater with an upper horizontal porous plate and a lower horizontal solid plate", *Ocean Eng.*, **35**, 1588-1596.

Losada, I.J., Silva, R. and Losada, M.A. (1996), "3-D non-breaking regular wave interaction with submerged breakwaters", *Coast. Eng. J.*, **28**(1-4), 229-248.

Mei, C.C. and Black, J.L. (1969), "Scattering of surface waves by rectangular obstacles in waters of finite depth", *J. Fluid Mech.*, **38**, 499-511.

Neves, M.G., Losada, I.J. and Losada, M.A. (2000), "Short-wave and wave group scattering by submerged porous plate" *J. Eng. Mech.*, **126**(10), 1048-1056.

Sollitt, C.K. and Cross, R.H. (1972), "Wave transmission through permeable breakwaters", *Proceedings of the 13th Coastal Engineering Conference*, Vancouver, Canada.

Twu, S.W., Liu, C.C. and Hsu, W.H. (2001), "Wave damping characteriscs of deeply submerged breakwaters", *J. Waterw. Port Coast. Ocean Eng.*, **127**(2), 97-105.

Wang, K.H. and Shen, Q. (1999), "Wave motion over a group of submerged horizontal plates", *Int. J. Eng. Sci.*, **37**, 703-715.

Wang, Y.X., Wang, G.Y. and Li, G.W. (2006), "Experimental study on the performance of the multiple-layer breakwater", *Ocean Eng.*, **33**, 1829-1839.

Yip, T.L. and Chwang, A.T. (1998), "Water wave control by submerged pitching porous plate", *J. Eng. Mech.*, **124**(4), 428-434.

Yu, X.P. (1995), "Diffraction of water waves by porous breakwaters", *J. Waterw. Port Coast. Ocean Eng.*, **121**(6), 275-282.

Yu, X.P. and Chwang, A.T. (1994), "Water waves above submerged porous plate", *J. Eng. Mech.*, **120**(6), 1270-1282.

Yueh, C.Y. and Chuang, S.H. (2009), "Wave scattering by a submerged porous plate wave absorber", *Proceedings of the 19th international offshore and polar engineering conference*, Osaka, Japan.

Appendix A

For symmetric problem, the seven sets of linear equations obtained by the second equals sign in Eq. (5) and Eqs. (6) and (7) are given by

$$[z_{nm}]\{E_m\} + [p_{nm}]\{F_m\} + [q_{nm}]\{B_m\} = [r_{nm}]\{A_m\} + [s_{nm}]\{D_m\} \tag{A.1}$$

$$[a_{nm}]\{A_m\} = [b_{nm}]\{R_m\} + [c_n] \tag{A.2}$$

$$\{B_n\} = [d_{nm}]\{R_m\} + [e_n] \tag{A.3}$$

$$\{C_n\} = [f_{nm}]\{R_m\} + [g_n] \tag{A.4}$$

$$\{h_m\} + \{R_m\} = [i_{mn}]\{A_n\} + [j_{mn}]\{B_n\} + [k_{mn}]\{C_n\} + [l_{mn}]\{D_n\}$$
$$+ [m_{mn}]\{E_n\} + [n_{mn}]\{F_n\} + [o_{mn}]\{G_n\} \tag{A.5}$$

$$\{E_n\} + [u_{nm}]\{B_m\} = [v_{nm}]\{G_m\} + [w_{nm}]\{C_m\} + [t_{nm}]\{F_m\} \tag{A.6}$$

$$\{G_n\} = [\tilde{a}_{nm}]\{F_m\} + [\tilde{b}_{nm}]\{E_m\} \tag{A.7}$$

where $n, m = 0, 1, 2,…, N$; and all the matrix coefficients in above equations are listed in Table A.1. For simplicity of expressions in Table A.1, the following functions are defined: $\tilde{k}_0 = -ik_0$; $\tilde{k}_m = k_m$ ($m \neq 0$); $\delta_{nm} = 0$ ($m \neq n$); $\delta_{nm} = 1$ ($m = n$); $U_0(\lambda_0 x) = \cos\lambda_0 x$; $U_0(\upsilon_0 x) = U_0(\mu_0 x) = 1$; $U_n(\alpha_n x) = \cosh\alpha_n x / \cosh\alpha_n b$ ($\alpha_n = \lambda_n, \upsilon_n$ and μ_n, $n = 1, 2, …$); $U_n'(-\lambda_n b) = dU_n(\lambda_n x)/dx\big|_{x=-b}$; $\tilde{Z}_m = \int_{-d}^{0}[Z_m(z)]^2\,dz$; $\tilde{W}_n = \int_{-b}^{0}[W_n(x)]^2\,dx$; $\tilde{Y}_n = \int_{-d_1}^{0}[Y_n(z)]^2\,dz$; $\tilde{V}_n = \int_{-d_2}^{-d_1}[V_n(z)]^2\,dz$ and $\tilde{X}_n = \int_{-d}^{-d_2}[X_n(z)]^2\,dz$.

Table A.1 Matrix coefficients in Eqs. (A.1) - (A.7).

Coefficients	Values	Coefficients	Values
a_{nm}	$\delta_{nm} U_n(\lambda_n b)$	p_{nm}	$\delta_{nm}\left[\tanh\beta_n a_1 - \beta_n/(ik_0 G)\right]$
$\tilde{a}_{nm}$	$\delta_{nm}/(\varepsilon\tanh\beta_n a)$	$\tilde{b}_{nm}$	$-\delta_{nm}\tanh\beta_n a_1/(\varepsilon\tanh\beta_n a)$
c_n	b_{n0}	d_{nm}	$\left.\int_{-d_2}^{-d_1} V_n(z)Z_m(z)\mathrm{d}z\right/\tilde{V}$
e_n	d_{n0}	f_{nm}	$\left.\int_{-d}^{-d_2} X_n(z)Z_m(z)\mathrm{d}z\right/\left[(s+\mathrm{i}f)\tilde{X}_n\right]$
g_n	f_{n0}	i_{mn}	$\left. U_n'(-\lambda_n b)\int_{-d_1}^{0} Z_m(z)Y_n(z)\mathrm{d}z\right/\left(\tilde{k}_m\tilde{Z}_m\right)$
h_m	$-\delta_{m0}$	j_{mn}	$\left. U_n'(-\upsilon_n b)\int_{-d_2}^{-d_1} Z_m(z)V_n(z)\mathrm{d}z\right/\left(\tilde{k}_m\tilde{Z}_m\right)$
b_{nm}	$\left.\int_{-d_1}^{0} Y_n(z)Z_m(z)\mathrm{d}z\right/\tilde{Y}_n$	k_{mn}	$\left.\varepsilon U_n'(-\mu_n b)\int_{-d}^{-d_2} Z_m(z)X_n(z)\mathrm{d}z\right/\left(\tilde{k}_m\tilde{Z}_m\right)$
v_{nm}	$\delta_{nm}(s+\mathrm{i}f)$	q_{nm}	$\left. V_m(-d)\int_{-b}^{0} W_n(x)U_m(\upsilon_m x)\mathrm{d}x\right/\tilde{W}_n$
t_{nm}	$\delta_{nm}\tanh\beta_n a_1$	w_{nm}	$\left.(s+\mathrm{i}f)X_m(-d_2)\int_{-b}^{0} W_n(x)U_m(\mu_m x)\mathrm{d}x\right/\tilde{W}_n$
z_{nm}	$\delta_{nm}\left[1-\beta_n\tanh(\beta_n a_1)/(ik_0 G)\right]$	s_{nm}	$\delta_{nm}\left[1-(K/\beta_n)\tanh\beta_n d_1\right]$
r_{nm}	$\left. Y_m(-d_1)\int_{-b}^{0} W_n(x)U_m(\lambda_m x)\mathrm{d}x\right/\tilde{W}_n$	u_{nm}	$\left. V_m(-d_2)\int_{-b}^{0} W_n(x)U_m(\upsilon_m x)\mathrm{d}x\right/\tilde{W}_n$

l_{mn}	$\left.\beta_n\sin\beta_n b\int_{-d_1}^{0} Z_m(z)\left[\cosh\beta_n z+(K/\beta_n)\sinh\beta_n z\right]\mathrm{d}z\right/\left(\tilde{k}_m\tilde{Z}_m\cosh\beta_n d_1\right)$
m_{mn}	$\left.\beta_n\sin\beta_n b\int_{-d_2}^{-d_1} Z_m(z)\cosh\beta_n(z+d_1+a_1)\mathrm{d}z\right/\left[\tilde{k}_m\tilde{Z}_m\cosh(\beta_n a_1)\right]$
n_{mn}	$\left.\beta_n\sin\beta_n b\int_{-d_2}^{-d_1} Z_m(z)\sinh\beta_n(z+d_1+a_1)\mathrm{d}z\right/\left[\tilde{k}_m\tilde{Z}_m\cosh(\beta_n a_1)\right]$
o_{mn}	$\left.\varepsilon\beta_n\sin\beta_n b\int_{-d}^{-d_2} Z_m(z)\cosh\beta_n(z+d)\mathrm{d}z\right/\left[\tilde{k}_m\tilde{Z}_m\cosh\beta_n a\right]$